Title

Tomographic imaging system for measuring impurity line emission in a field-reversed configuration[a)]

Journal

Review of Scientific Instruments, 83(10)

ISSN

0034-6748

Authors

Roche, T

Bolte, N

Garate, E

et al.

Publication Date

2012-10-01

DOI

10.1063/1.4729670

Tomographic imaging system for measuring impurity line emission in a field-reversed configuration[a)]

T. Roche,[1,b)] N. Bolte,[1,2] E. Garate,[1,2] W. W. Heidbrink,[1] R. McWilliams,[1] and F. Wessel[1,2]
[1]*University of California, Irvine, California 92697, USA*
[2]*Tri Alpha Energy, Inc., Rancho Santa Margarita, California 92688, USA*

(Presented 7 May 2012; received 6 May 2012; accepted 28 May 2012; published online 20 June 2012)

A 16 chord optical tomography system has been developed and implemented in the flux coil generated-field reversed configuration (FRC). The chords are arranged in two fans of eight, which cover ∼35% of the vessel area at the midplane. Each illuminate separate photomultiplier tubes (PMTs) which are fitted with narrow band-pass filters. In this case, filters are centered at 434.8 nm to measure emission from singly ionized argon. PMT crosstalk is negligible. Background noise due to electron radiation and H_γ line radiation is <10% of argon emission. The spatial resolution of the reconstruction is 1.5 cm. Argon is introduced using a puff valve and tube designed to impart the gas into the system as the FRC is forming. Reconstruction of experimental data results in time-dependent, 2D emissivity profiles of the impurity ions. Analysis of these data show radial, cross-field diffusion to be in the range of 10–10^3 m^2/s during FRC equilibrium. © *2012 American Institute of Physics*. [http://dx.doi.org/10.1063/1.4729670]

I. INTRODUCTION

Complete understanding of transport processes occurring in a field-reversed configuration (FRC) is essential for long timescale confinement.[1] Injection of impurity species into plasma can lead to measurement of localized particle flux/diffusion through line emission observation. Reconstruction of these data gives 2D, time evolved emissivity profiles. Analysis of profiles provides direct measurement of $D_\perp$ of the impurity species, which contributes to overall understanding of plasma transport processes. These values can be compared to theoretical predictions, which, until now, have had to rely on inferential measurements in hydrogen FRCs.

II. EXPERIMENTAL SETUP

A. Flux-coil generated-field reversed configuration (FCG-FRC) device

The FCG-FRC is a cylindrical device where an FRC is formed between two concentric sets of coils. Gota *et al.*,[2] Gupta *et al.*,[3] and Slepchenkov *et al.*[4] describe this device in more detail. Inner solenoid (flux-coil) is encased in a quartz tube with outer diameter 17.1 cm which defines the inner boundary of the vacuum vessel. Outer boundary of the vacuum chamber consists of two, coaxial pyrex tubes of diameter 61.4 cm which sandwich a polyethylene block capable of supporting many diagnostics. Total length of system is 2.1 m. 16 outer coils are dispersed axially along machine at $r = 42$ cm. They provide the confining magnetic field. Currents in coils can be controlled independently.[4] A large (60 kA) current in the flux-coil induces a comparable plasma current, which reverses the magnetic field, establishing the FRC.[5,6] Resulting magnetic fields are around ±200 G.

B. Hardware setup

The basic design principle for the tomography diagnostic consists of 2 fan arrays with 8 collimated lines of sight each. The light incident on each collimator lens is focused onto a fiber, which transmits light through a series of filters, and is finally measured by 1 of 16 photomultiplier tubes (PMTs). General setup of light collection apparatus is shown in Fig. 1. We are limited to 2 views by space constraints; all other ports are in use by other diagnostics.

Collimators are cylindrical in shape (Fig. 2). They have outer diameters of 1 cm, inner diameters of 0.4 cm and length of ∼3 cm. They are constructed out of high density polyethylene (HDPE). In total, each collimator consists of 2 threaded cylinders, 2 retaining rings, and a lens. The lens is Thorlabs Inc. part number LA1222. It is composed of BK-7 glass with outer diameter of 0.6 cm and focal length 1.36 cm. As the entrance orifice is only 0.4 cm in diameter, only the central portion of the lens in illuminated during experimentation. This reduces spherical aberration and acceptance angle, both of which improve the collimation. The collimator has an acceptance angle of ∼1°; so the spot size, in plasma, is smaller than pixels in the reconstruction. This makes the line integral approximation appropriate. These components were modeled with ZEMAX. The back side of the collimator is threaded such that a standard SubMiniature version A (SMA) fiber optic connector can be attached to it. The two pieces making up the body of the collimator can be adjusted so that the light passing through the lens is focused directly onto fiber.

Optical fan arrays were designed to fit seamlessly into central HDPE block through two diagnostic slots (Fig. 1).

[a)]Contributed paper, published as part of the Proceedings of the 19th Topical Conference on High-Temperature Plasma Diagnostics, Monterey, California, May 2012.

[b)]Author to whom correspondence should be addressed. Electronic mail: troche@uci.edu.

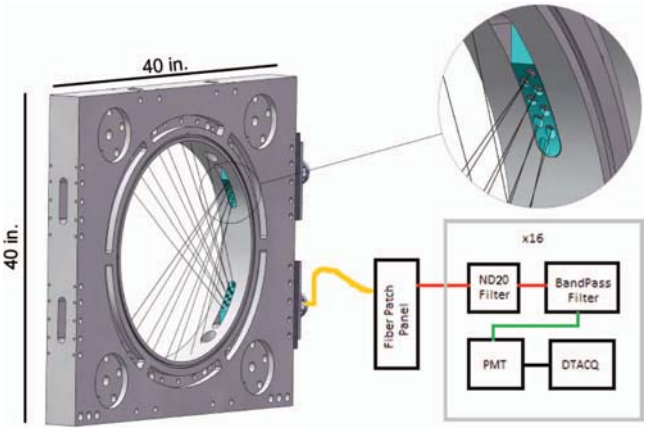

FIG. 1. Schematic of tomographic diagnostic.

Each fan has holes drilled for 8 collimators and screws to secure them. Each views the plasma at a different angle ranging from 37.79° to 71.04°. Resulting line of sight coverage is displayed in Fig. 1. Fan array is held in place by 2 supporting rods which connect to a stainless steel flange. The flange is designed to interface with the machine's vacuum system (Fig. 1) and is fitted with a 2 3/4 in. conflat receptacle for the fiber optic feedthru.

Broad spectrum light produced by plasma has many sources: emitting ions, emitting neutrals, and radiating electrons to name a few. Since the interest of this experiment is to observe transport of impurity ions, optical filters are necessary to select radiation from desired line emission. Argon was chosen as the impurity species at ∼1% of the mostly nitrogen plasma. The selected line has a wavelength of 434.8 nm. Therefore, optical band-pass filters are installed in-line between the fiber optic cable and the PMTs. The filters themselves are 1/2 in. in diameter and have an acceptance window of ∼1 nm. Even after this filtration the intensity of the line emission is still great enough to saturate PMTs, so additional neutral density (ND20) filters are added to reduce the intensity to measurable levels.

Chamber reflections, including diffusive, have reflection coefficients <0.04. Considering spatial geometry of imaged features and reflecting surface shapes indicates reflections contribute <0.01% to the signal, well below other noise sources. Also, ghost features were not observed in the reconstructions.

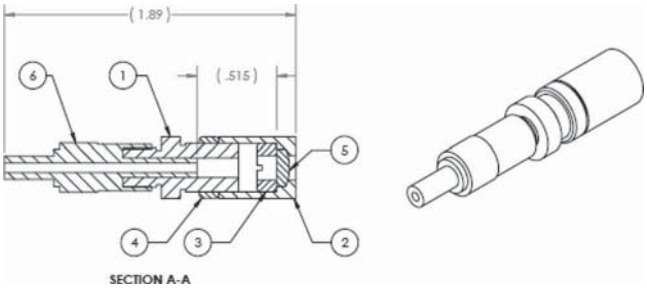

FIG. 2. Schematic of optical collimators used in experiment. Dimensions in inches. (1) SMA mount, (2) lens mount, (3) lens mount ring, (4) SMA mount ring, (5) Thorlabs LA1222, (6) 905 polymide fiber connector 600 μm.

Chord sensitivities are calibrated, relative to each other, by coupling a light emitting diode (LED) directly to fiber optic. The LED's emissivity spectrum is broad enough so that there is plenty of light in the 434.8 ± 1 nm range. LED is pulsed (to avoid PMT saturation) and PMT's response is recorded. This is done for each of the 16 chords, then output voltages are normalized. Normalized values are used as calibration factors.

III. RECONSTRUCTION ALGORITHM

Inversion technique employed in this work is called minimum Fisher regularization. It was developed by Anton *et al.*[7] as a hybrid of linear regularization (LR) and minimum Fisher information (MFI). The basic idea is to solve the following set of equations:

$$f_l = \int_{S_l} \mathrm{d}s\ g(\boldsymbol{r}) \qquad l = 1 \ldots n_l, \tag{1}$$

where the f_l are the (relatively) calibrated PMT signals and $g(\boldsymbol{r})$ is the emissivity of the plasma. We discretize $\boldsymbol{g}$ by breaking the space into square pixels. There are n_x pixels in the horizontal direction and n_y pixels in the vertical direction for a total of $n_{pixels} = n_x \times n_y$. $\boldsymbol{g}$ and $\boldsymbol{f}$ become column vectors with n_{pixels} and n_l rows, respectively. Then, Eq. (1) becomes

$$\boldsymbol{f} = \mathbf{T} * \boldsymbol{g}, \tag{2}$$

where $\mathbf{T}$ is a matrix which contains the geometric information of the lines of sight, such that

$$T_{li} = \int_{S_{li}} \mathrm{d}s. \tag{3}$$

In other words, T_{li} represents the length of chord l inside pixel i. Generally speaking, direct inversion of $\mathbf{T}$ is not possible. Either there are too few equations, i.e., $\mathbf{T}$ is not invertible or, even if we had $n_{pixels} = n_l$, $\mathbf{T}$ is poorly conditioned (very sparse). This is where LR comes in. We add a smoothing matrix which couples adjacent pixels. In 2nd order LR, the matrix is the finite-difference Laplacian.[7] Incorporating the LR matrix and Eqs. (2) and (3) we seek to minimize

$$\phi = \tfrac{1}{2}(\tilde{\mathbf{T}} * \boldsymbol{g} - \tilde{\boldsymbol{f}})^{\mathrm{T}} * (\tilde{\mathbf{T}} * \boldsymbol{g} - \tilde{\boldsymbol{f}}) + \boldsymbol{g}^{\mathrm{T}} * \mathbf{H} * \boldsymbol{g}, \tag{4}$$

where ϕ is χ^2 for the system with the smoothing matrix, $\mathbf{H}$, incorporated. The tildes represent division by the standard deviation of f_l, i.e., $\tilde{f}_l = f_l/\sigma_l$. Reconstructing the most accurate image requires that contributions from the chord geometry ($\mathbf{T}$ matrix) and the system geometry (LR matrix) must be weighted for each pixel individually. This weighting procedure is the MFI portion of the algorithm.[7] The weights are determined by Eq. (5) through successive iterations of the reconstruction process.

$$W_{ij}^{(n)} = \begin{cases} \frac{1}{2\, g_i^{(n)} g_i^{(n-1)}} \cdot \delta_{ij} & g_i^{(n)} > 0 \quad n > 0 \\ W_{\max} \cdot \delta_{ij} & g_i^{(n)} \le 0 \quad n > 0 \end{cases} \tag{5}$$

$W_{\max}$ is a maximum weighting value used for those pixels which have erroneously been determined to be negative. $W_{\max}$ is simply $1/g_{\min}$ for $g_i > 0$. The smoothing matrix becomes,

$$\mathbf{H} \to \mathbf{H}^{(n)} = \Delta^{\mathrm{T}} * \mathbf{W}^{(n)} * \Delta, \tag{6}$$

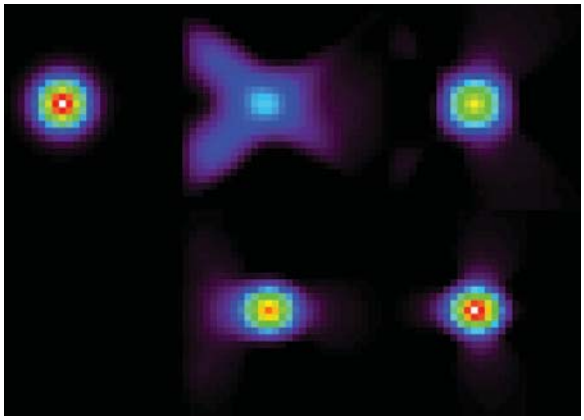

FIG. 3. Simulation with Gaussian input. Top left: Input image. Then from left to right, top to bottom: successive iterations of the algorithm. Notice how the iterative weighting recovers not only the shape, but the peak height of the input.

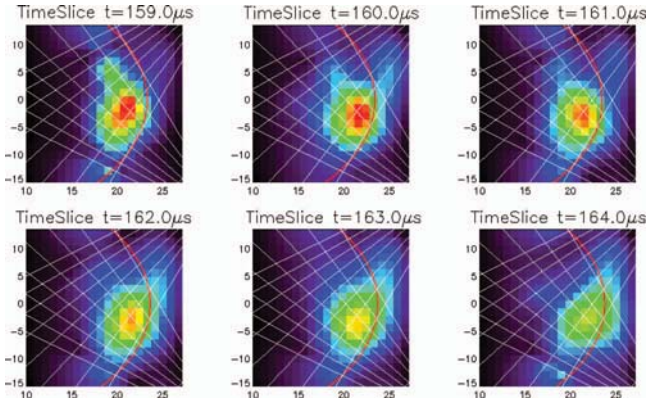

FIG. 5. Reconstructed density profiles during FRC equilibrium at 1 μs time steps. The units of both axes are centimeters. The white lines represent the 16 collimated lines of sight. The red arcs represent the position of the magnetic null at the depicted time slices.[1]

This leads us to the system of equations to be solved,

$$(\tilde{\mathbf{T}}^{\mathrm{T}} * \tilde{\mathbf{T}} + \mathbf{H}^{(n)}) * \boldsymbol{g}^{(n+1)} = \tilde{\mathbf{T}}^{\mathrm{T}} * \tilde{\boldsymbol{f}}, \tag{7}$$

where we have set all of the $\partial\phi/\partial g_i = 0$. A more complete derivation of these equations is available in Anton *et al.*[7] The number of iterations that must be performed was determined by looking at successive reconstructions of simulated input data as shown in Fig. 3. The reconstructions converged after 4 iterations.

IV. EXPERIMENTAL DATA

Raw signals from a typical shot are displayed in Fig. 4. The signals have been adjusted by their associated calibration factors. Inverting the data at 1 μs intervals yields 2D images of the reconstruction area as shown in Fig. 5. The data presented are typical during FRC equilibrium. The FRC is very stable during this 20–30 μs time window.

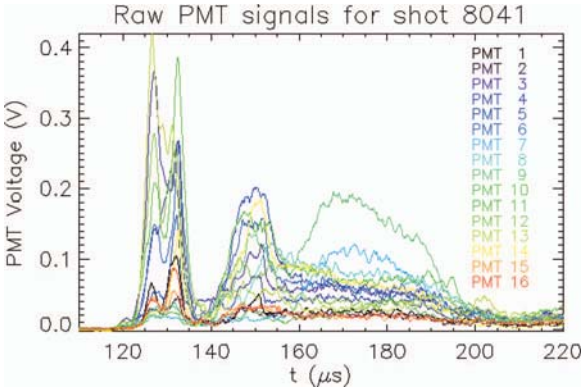

FIG. 4. Signals from PMTs preinversion.

V. SUMMARY AND DISCUSSION

The design of a new tomographic apparatus was described. Its analysis methodology was explained and verified. Reconstruction of experimental data show the emissivity profile as a function of time for an FRC. Further analysis of these data show they represent the impurity density profile. This information has led to the preliminary calculation of the plasma's diffusion coefficient of 10–10^3 m^2/s.

[1] L. C. Steinhauer, Phys. Plasmas **18**, 070501 (2011).
[2] H. Gota, N. Bolte, B. Deng, D. Gupta, V. Kiyashko, K. Knapp, R. Mendoza, M. Morehouse, T. Roche, and F. Wessel, Rev. Sci. Instrum. **81**, 10D512 (2010).
[3] D. Gupta, N. Bolte, H. Gota, R. Hayashi, V. Kiyashko, P. Marsili, M. Morehouse, S. Primavera, T. Roche, and F. Wessel, Rev. Sci. Instrum. **81**, 10D730 (2009).
[4] M. Slepchenkov, M. Morehouse, V. Kiyashko, F. Wessel, N. Rostoker, N. Bolte, and T. Roche, in *2011 IEEE/NPSS 24th Symposium on Fusion Engineering (SOFE)* (2011), pp. 1–5.
[5] Z. Pietrzyk, G. Vlases, R. Brooks, K. Hahn, and R. Raman, Nucl. Fusion **27**, 1478 (1987).
[6] W. Pierce, R. Maqueda, R. Brooks, and R. Farengo, Nucl. Fusion **33**, 117 (1993).
[7] M. Anton, H. Weisen, M. J. Dutch, W. vonderLinden, F. Buhlmann, R. Chavan, B. Marletaz, P. Marmillod, and P. Paris, Plasma Phys. Controlled Fusion **38**, 1849 (1996).